

## The *RARS-MAD1L1* Fusion Gene Induces Cancer Stem Cell-like Properties and Therapeutic Resistance in Nasopharyngeal Carcinoma

Qian Zhong<sup>#1</sup>, Zhi-Hua Liu<sup>#1,2</sup>, Zhi-Rui Lin<sup>#1</sup>, Ze-Dong Hu<sup>3</sup>, Li Yuan<sup>1</sup>, Yan-min Liu<sup>1</sup>, Ai-Jun Zhou<sup>1</sup>, Li-Hua Xu<sup>4</sup>, Li-Juan Hu<sup>5</sup>, Zi-feng Wang<sup>1</sup>, Xin-Yuan Guan<sup>1</sup>, Jia-Jie Hao<sup>6</sup>, Vivian W.Y. Lui<sup>7</sup>, Ling Guo<sup>1,8</sup>, Hai-Qiang Mai<sup>1,8</sup>, Ming-Yuan Chen<sup>1,8</sup>, Fei Han<sup>1,8</sup>, Yun-Fei Xia<sup>1,9</sup>, Jennifer R. Grandis<sup>10</sup>, Xing Zhang<sup>\*1</sup>, Mu-Sheng Zeng<sup>\*1</sup>

1: State Key Laboratory of Oncology in South China, Collaborative Innovation Center for Cancer Medicine, Sun Yat-Sen University Cancer Center

2: Innovation Center of Cancer Medicine, National Institute of Biological Sciences, Beijing, China

3: Department of Pain Treatment, the Fourth People's Hospital of Kunming city, Yunnan, China

4: Department of Oncology and Hematology, The First Affiliated Hospital of Guangzhou Medical University, Guangzhou, China

5: Peking University People's Hospital and Peking University Institute of Hematology, Beijing Key Laboratory of Hematopoietic Stem Cell Transplantation, Beijing 100044, China

6: State Key Laboratory of Molecular Oncology, National Cancer Center/Cancer Hospital, Chinese Academy of Medical Sciences and Peking Union Medical College, Beijing, China

7: School of Biomedical Sciences, Faculty of Medicine, The Chinese University of Hong Kong, Shatin, Hong Kong SAR

8: Department of Nasopharyngeal Carcinoma, Sun Yat-Sen University Cancer Center,  
Guangzhou, China

9: Department of Radiation Oncology, Sun Yat-Sen University Cancer Center, Guangzhou,  
China

10: Department of Otolaryngology Head and Neck Surgery and Clinical and Translational  
Science Institute, University of California at San Francisco, San Francisco, CA, USA

#: These authors contributed equally to this work

\*:Co-corresponding authors: Xing Zhang and Mu-Sheng Zeng

Running title: The Oncogenic Role of *RARS-MAD1L1* in NPC

Key words: Fusion Gene, *RARS-MAD1L1*, Tumorigenicity, Therapeutic  
Resistance, Nasopharyngeal Carcinoma

## Abstract

**Background:** Nasopharyngeal carcinoma (NPC) is most common head and neck cancer in Southeast Asia. Because local recurrence and distant metastasis are still the main causes of NPC treatment failure, it is urgent to identify new tumor markers and therapeutic targets for advanced NPC.

**Methods:** RNA-seq was applied to look for interchromosome translocation in NPC. PCR, FISH and immunoprecipitation were used to examine the fusion gene expression at RNA, DNA, and protein levels in NPC biopsies. MTT assay, colony formation assay, sphere formation assay, co-IP, ChIP assay, and *in vivo* chemoresistance assay were applied to explore the function of *RARS-MAD1L1* in NPC.

**Results:** We demonstrated that *RARS-MAD1L1* was present in 10.03% (35/349) primary NPC biopsies and 10.7% (9/84) in head and neck cancer (HNC) samples. *RARS-MAD1L1* overexpression increased cell proliferation, colony formation, and tumorigenicity *in vitro*, and the silencing of endogenous *RARS-MAD1L1* reduced cancer cell growth and colony formation *in vitro*. Additionally, *RARS-MAD1L1* increased the side population (SP) ratio and induced chemo- and radio-resistance. Furthermore *RARS-MAD1L1* interacted with AIMP2, which resulted in activation of FUBP1/c-Myc pathway. The silencing of FUBP1 or the administration of a c-Myc inhibitor abrogated the cancer stem cell (CSC)-like characteristics induced by *RARS-MAD1L1*. The

expression of c-Myc and ABCG2 was higher in *RARS-MAD1L1* positive HNC samples than in negative samples.

**Conclusion:** Our findings indicate that *RARS-MAD1L1* might contribute to tumorigenesis, CSC-like properties and therapeutic resistance, at least in part, through the FUBP1/c-Myc axis, implying that *RARS-MAD1L1* might serve as an attractive target for therapeutic intervention for NPC.

**Statement of Significance:**

This study demonstrated that a fusion gene, *RARS-MAD1L1*, was present in primary nasopharyngeal carcinoma and head & neck cancer biopsies and induces cellular proliferation and cancer stem-cell properties in NPC. The FUBP1/c-Myc axis was activated by *RARS-MAD1L1*. These data indicate that the development of drugs targeting this axis via combinatorial therapy might benefit patients carrying this fusion gene.

## Introduction

Nasopharyngeal carcinoma (NPC) is a common malignant epithelial tumor of the nasopharynx in Southeast Asia with high invasive and metastatic potential. The incidence of NPC is 27.2/100,000 among males and 11.3/100,000 among females in a high-risk area of South China (1, 2). Although NPC is sensitive to radiotherapy, the main causes of NPC treatment failure are local recurrence and distant metastasis (3, 4). Therefore, the identification of new tumor markers and therapeutic targets for advanced NPC is urgently needed.

Genome instability, as one of the hallmarks of cancer, might account for gene mutations, alterations in chromosome number, gene amplifications and chromosome translocations (5). In NPC biopsies, loss of heterozygosity in chromosomes 3p, 9p, 9q, 11q, 13q, 14q, and 16q (6-8) and gain regions in chromosomes 1q, 3q, 8q, 12, and 20q (6, 9) have been frequently observed. Alterations in the chromosome number in NPC have been shown to correlate with NPC progression (6).

Fusion genes as a result of chromosomal translocation, inversion or deletion serve as therapeutic targets for many types of cancer (10). The first characterized fusion gene, BCR-ABL, which is caused by the Philadelphia translocation, is present in most chronic myelogenous leukemia (CML) cases (11), and treatment with imatinib to inhibit the BCR-ABL tyrosine kinase has

revolutionized treatment for CML patients (12). In solid tumors, the TMPRSS2-ERG fusion gene serves as a prognostic marker of prostate cancer (13). EML4-ALK was identified in non-small cell lung cancer (NSCLC) (14), and crizotinib, which targets EML4-ALK, is associated with a better clinical response (15).

In NPC, several fusion genes, including *FGFR3-TACC3* (16), *UBR5-ZNF423*, *CTAGE5-PSMA3* and *RARS-MAD1L1* (17), have been identified by RNA-Seq. We previously detected the presence of the *FGFR3-TACC3* fusion gene in approximately 2-4% of NPC, head and neck squamous cell carcinoma, esophageal squamous cell carcinoma and lung cancer samples (16). *FGFR3-TACC3* has been shown to induce oncogenic characteristics by activating FGFR kinase activity and is a potential therapeutic target (16, 18). *UBR5-ZNF423* was identified in the C666-1 NPC cell line and in 12/144 NPC tissues. A function analysis has suggested that *UBR5-ZNF423* might play an important role in tumorigenesis in a subset of NPC cases. Whether *UBR5-ZNF423* represents a therapeutic target in NPC needs further investigation (17). Although Chung *et al.* reported several other fusion transcripts, including *RARS-MAD1L1*, in C666-1 cells (17), we provide the first characterization of *RARS-MAD1L1* as a recurrent fusion in approximately 10% of primary NPC tumors and head and neck cancer cases. Furthermore, we demonstrated that *RARS-MAD1L1* might contribute to tumorigenesis and

therapeutic resistance by inducing cancer stem cell (CSC)-like properties in NPC.

## **Materials and Methods**

### **Patients and specimens**

All clinical samples used for the quantitative RT-PCR and fluorescence *in situ* hybridization (FISH) assays of RARS-MAD1L1 expression were collected from Sun Yat-Sen University Cancer Center (SYSUCC), Guangzhou, China. A total of 349 NPC biopsy specimens and 84 in-patient HNC biopsies were collected in 2011 for reverse-transcription PCR assays. For FISH analysis, eight biopsy specimens and two paraffin-embedded NPC specimens were collected. Eighty-four in-patient HNC patients samples, which were histologically and clinically diagnosed in patients with radical surgery in SYSUCC between 2010 and 2011, were included in this study. All the NPC biopsies from SYSUCC and YunNan Province Cancer Hospital were histologically diagnosed. The informed consent was obtained from each patient prior to surgery and the study was approved from the Institute Research Ethics Committee. Each biopsy specimen was immersed in RNA Later reagent overnight at 4°C and then preserved at -80°C until RNA extraction. All the patients were followed from the date of diagnosis until death or the lasted census date. The characteristics of 84 HNC patients were included in supplemental table 1.

## **Antibodies and reagents**

Antibodies against the C-terminal region of MAD1L1 (Cat# A300-355A) were purchased from Bethyl Laboratories (Montgomery, TX, USA). The following additional antibodies were used: against the N-terminal region of RARS (Novus Biologicals, Littleton, CO, USA, cat# PAB28524), Flag M2 (Sigma-Aldrich, St. Louis, MO, USA, cat# F1804), AIMP2 (Abcam, Cambridge, MA, USA, cat#F1804),  $\beta$ -actin (Proteintech Group Inc., Rosemont, IL, USA, cat#66009-1-1g), ABCG2 (Abcam, Cambridge, UK, cat# ab3380), Sox2 (Cell Signaling, Danvers, MA, USA, cat#3579), c-Myc (Cell Signaling, cat#5605s), Bmi-1 (Cell Signaling, cat#2933), FUBP1 (Abcam, cat#213528)  $\alpha$ -tubulin (Cell Signaling, cat#2125s), glyceraldehyde-3-phosphate dehydrogenase (GAPDH) (KangChen Biotech, Shanghai, China, cat#60004), and Texas Red®-X-conjugated wheat germ agglutinin (WGA) (Thermo Fisher, Waltham, MA, USA, cat#11262), FITC-conjugated anti-rabbit IgG (Invitrogen, Carlsbad, CA, USA). The Myc inhibitor (10058-F4) and fumitremorgin C (FTC) were purchased from Selleck Chemicals (Houston, TX, USA, cat#s7153) and Sigma-Aldrich (SKBO), respectively. Cisplatin (DDP) and 5-fluorouracil (5-FU) were obtained from Hospira Australia Pty., Ltd. (Lexia Place, Australia).

## **FISH analysis**

FISH analysis of fresh tumor tissues or paraffin-embedded tissue specimens was conducted using a previously described method (19-21).

### **Cell lines and culture conditions**

The NPC cell lines CNE2, HK1, and S26 were cultured in RPMI-1640 (Invitrogen, USA) supplemented with 5% fetal bovine serum (FBS) (Invitrogen). C666-1, another NPC cell line, was cultured on CellBIND culture flasks (Corning Inc., NY, USA) in RPMI-1640 supplemented with 10% FBS. Additionally, p53<sup>-/-</sup> mouse embryonic fibroblasts (MEFs) and 293T cells were cultured in DMEM (Invitrogen) supplemented with 10% FBS. All cell lines were cultured in a humidified incubator containing 5% CO<sub>2</sub> at 37°C. Cell line authentication was performed according to the suggestions from ATCC cell line authentication (supplementale table 2). CNE2 and HNE1 cell lines are possibly contaminated with Hela but HK1 and C666-1 cells are not contaminated. All the cells were tested for mycoplasma contamination.

### **Plasmid construction, retrovirus infection, and establishment of stable cell lines**

RARS-MAD1L1 was amplified from C666-1 cell cDNA and then subcloned into the pBabe vector to generate pBabe-RARS-MAD1L1. Retrovirus was produced as described previously (16). CNE2 cells, HK1, S26 cells and MEFs were infected with retrovirus carrying RARS-MAD1L1 or pBabe (empty vector). CNE2 cells, HK1 cells, S26 cells or MEFs expressing RARS-MAD1L1 or empty vector were selected with puromycin (Sigma-Aldrich, St. Louis, MO,

USA cat#101-58-58-2) for seven days after infection. After 10 days of selection, the generation of RARS-MAD1L1-expressing and empty vector-harboring stable cell lines was verified, and the resulting cells were cultured in fresh medium.

### **Treatment of NPC cells**

RARS-MAD1L1-expressing or pBabe (empty vector)-carrying stable CNE2, HK1, S26, or MEFs cells were seeded in 96-well plates at a density of  $2 \times 10^3$  cells/well. The next day, the cells were treated with various concentrations of DDP or 5-FU for 48 h to determine the concentration of each drug inhibition 50% growth ( $IC_{50}$ ) in these cell lines. To examine the sensitivities to 5-FU upon ko143 treatment, CNE2-RARS-MAD1L1 and CNE2-vector was pretreated with 10  $\mu$ M Ko143 or DMSO, then treated with 5-FU at 0.3  $\mu$ g/ml in the presence of 10  $\mu$ M Ko143 or DMSO (Sigma) for 48 hr. Alternatively, stable CNE2 and HK1 cells were seeded in six-well plates at a density of  $1 \times 10^3$ , cultured for 48 h, and irradiated once with one of five different doses (2, 4, 6, 8 or 10 Gy) of X-irradiation at room temperature using an RS2000 irradiator (Rad Source Technologies Inc., Suwanee, GA, USA). The cells were then cultured for 10 days to allow for colony formation.

The stable CNE2 cells were seeded at  $1.5 \times 10^5$  cells/well in a six-well plate and were then treated with 100  $\mu$ M 10058-F4, an inhibitor of c-Myc, or DMSO on

the following day. After 48 h, the cells were harvested for further experiments, including qRT-PCR, Western blotting, and SP ratio analyses. For mRNA half-life assessment in cell lines, actinomycin D (ACTD, 5ug/ml, Selleck) was added after 48h, cells were cultured and RNA was prepared at the indicated times.

### **Transfection with siRNA**

Transient transfection of C666-1 cells was performed using Lipofectamine™ RNAiMax (Invitrogen, Carlsbad, CA, USA, cat#1795160) according to the manufacturer's instructions. C666-1 cells were seeded at  $2 \times 10^5$  cells/well in a six-well plate one day prior to transfection. The following day, cells were transfected with 40 pmol siRNA and then subjected to CCK8 and soft-agar assays at 24 h post-transfection. Scramble siRNA was purchased from Ruibo (Guangzhou, China). The siRNA list were included in the supplemental Methods and Materials.

### ***In vivo* chemoresistance assay**

Four- to six-week-old female BALB/c nude mice (n=28) were purchased from Shanghai Slac Laboratory Animal Co., Ltd. (Shanghai, China) and maintained in Micro-Isolator cages. The animal experiments were approved by The Institutional Animal Care and Use Committee at Sun Yat-sen Cancer Center. All 28 mice were randomly assigned to four groups and underwent

subcutaneous injection of 100  $\mu$ l of a viable cell suspension mixture ( $2 \times 10^6$ ) containing 75% vector-harboring or RARS-MAD1L1-expressing CNE2 cell suspension and 25% Matrigel. When a tumor formed, the mice were subjected to different treatments (the control group was administered NaCl (200  $\mu$ l), and the experimental group was administered DDP (4 mg/kg)) continuously for 10 days. The tumor size was measured using calipers daily. All mice were sacrificed on the day after drug withdrawal.

### **Statistical analyses**

All data were analyzed using SPSS standard version 16.0 (SPSS, Chicago, IL, USA) and GraphPad Prism version 5.0 (GraphPad Software, San Diego, CA, USA). The data are presented as the means  $\pm$  S.E.M. from at least three independent experiments. All tests were two sided. The variance among the comparison groups was verified to be equivalent. The survival analysis was analyzed by the log-rank test. The comparison between two groups was analyzed by Student's t-test. When comparing more than two groups, one-way ANOVA or two-way ANOVA followed by the Bonferroni post-hoc test was performed. No animals or samples were excluded from the study. No statistical methods were used to determine the sample size. The *in vivo* experiments were not blinded. A P-value less than 0.05 was considered significant: \*,  $p < 0.05$ ; \*\*,  $p < 0.01$ , and \*\*\*,  $p < 0.001$ .

## Results

### Identification of *RARS-MAD1L1* in NPC

To identify novel fusion genes in NPC, we performed paired-end RNA-Seq in the C666-1 NPC cell line and on primary nasopharyngeal epithelial cells (NPECs). We identified an interchromosomal fusion of exons 1-7 of the plus strand of arginyl-tRNA synthetase (*RARS*) on Chr 5q34 to exon 19 of the minus strand of mitotic arrest deficient 1-like protein 1 (*MAD1L1*) on Chr7p22.3 (Supplemental Figure 1A).

### Characterization of the *RARS-MAD1L1* genomic rearrangement in C666-1 cells

To examine whether the *RARS-MAD1L1* fusion resulted from a genomic DNA rearrangement, we performed a FISH assay. Two paired sets of *RARS* and *MAD1L1* probes were designed, and the target sites of these probes are shown in Figure 1A. Although no fusion of the *RARS* and *MAD1L1* probes was observed in normal peripheral blood cells, the *RARS-MAD1L1* fusion was detected as yellow dots in C666-1 cells according to two separate paired sets of *RARS* and *MAD1L1* probes tested in two different laboratories (Figure 1B). These results confirmed that the *RARS-MAD1L1* fusion gene resulted from a genomic rearrangement. We then performed long-range PCR to analyze the breakpoint of the *RARS-MAD1L1* fusion at the genomic DNA level. We designed two specific primers for intron 6 of the *RARS* gene and one primer for

the 3' UTR of exon 19 of *MAD1L1*, and the amplified PCR products were analyzed by Sanger sequencing. As shown in Figure 1C and supplemental data 1, an ~8.4-kb DNA fragment corresponding to a portion of *HDAC9* intron 9 (positions 18268256-18276625 on Chromosome 7) was inserted between the *RARS* gene (position 167926434) on Chromosome 5 and the *MAD1L1* gene (position 1880783) on Chromosome 7.

We further analyzed the 5' and 3' UTRs of the *RARS-MAD1L1* fusion gene in C666-1 cells using 5' and 3' RACE. The sequencing results are shown in Supplemental data 2. Two versions of the 3' UTR of the full-length *RARS-MAD1L1* fusion gene were detected.

### **Detection of *RARS-MAD1L1* protein expression**

According to the sequence of the fusion gene *RARS-MAD1L1*, the predicted fusion protein contained major parts of the *RARS* protein and part of the *MAD1L1* C-terminal domain (CTD) (Figure 1D). The endogenous expression of the *RARS-MAD1L1* protein in C666-1 cells was detected by Western blotting (Figure 1E) and immunoprecipitation (Figure 1F) using HeLa or 293T cells transfected with the *RARS-MAD1L1* fusion gene as a positive control.

### **Detection of *RARS-MAD1L1* in NPC**

To evaluate the occurrence rate of *RARS-MAD1L1* in NPC, we examined *RARS-MAD1L1* expression in fresh NPC biopsy specimens by reverse-transcription PCR. We found that 35 of the 349 NPC tissues examined (10.03%) (Figure 1G and Supplemental Figure 1B) and 9 of the 84 head and neck cancer tissues (10.7%) were positive for *RARS-MAD1L1*, indicating that this *RARS-MAD1L1* fusion creates an in-frame transcript. However, *RARS-MAD1L1* expression was not correlated with other clinical parameters, likely due to the limited sample size (Supplemental Table 1). To confirm this genomic rearrangement in NPC tissues detected with *RARS-MAD1L1*, we collected eight NPC biopsy specimens (Figure 1H) and two formalin-fixed paraffin-embedded (FFPE) NPC specimens (Figure 1I) and performed FISH analysis on these specimens using two paired sets of *RARS* and *MAD1L1* probes. We detected a positive fusion signal in these eight fresh PCR-positive NPC biopsies and two examined FFPE PCR-positive NPC specimens. These results confirmed the occurrence of the *RARS-MAD1L1* fusion gene in NPC patients.

### **Oncogenic potential of *RARS-MAD1L1* in NPC**

To explore the role of *RARS-MAD1L1* in NPC, we generated CNE2 cell lines, p53<sup>-/-</sup> MEF lines, and S26 cell lines stably expressing *RARS-MAD1L1* or an empty vector via retroviral infection. We confirmed the successful establishment of these cell lines (Figure 2A and Supplemental Figures 2A and

2D). The RARS-MAD1L1-expressing CNE2 cells, MEFs and S26 cells grew faster (Figure 2B and Supplemental Figures 2B and 2E) and formed more colonies in colony-formation assays than the control cells (Figure 2C and Supplemental Figures 2C and 2F). Furthermore, an anchorage-independent growth assay showed that RARS-MAD1L1-expressing CNE2 cells and S26 cells formed more and larger colonies than the empty vector-infected cells (Figure 2D and Supplemental Figure 2G). These results indicate that the RARS-MAD1L1 fusion gene enhances cell transformation abilities.

We also examined the oncogenic role of *RARS-MAD1L1* in C666-1 cells by silencing *RARS-MAD1L1* in C666-1 cells using siRNAs. Due to the low knock-down efficiency of siRNAs targeting the *RARS-MAD1L1* breakpoint, we designed nine siRNAs and selected four of them for further experiments due to their higher specificity against the *RARS-MAD1L1* fusion gene, the RARS wild-type gene or the MAD1L1 wild-type gene. These four specific siRNAs were as follows: siRNA-RARS-001 (siRARS-001), targeting only wild-type *RARS*; siRNA-RARS-005 (siRARS-005), targeting both wild-type *RARS* and the *RARS-MAD1L1* fusion gene; siRNA-MAD1L1-002 (siMAD1L1-002), targeting only wild-type *MAD1L1*; and siRNA-MAD1L1-003 (siMAD1L1-003), targeting both the wild-type *MAD1L1* and the *RARS-MAD1L1* fusion gene. Twenty-four hours after transfection with these siRNAs, the C666-1 cells were plated for CCK8 and colony-formation assays. As shown in Figures 2E, 2F,

and 2G, the silencing of *RARS-MAD1L1* using siRARS-005 or siMAD1L1-003 significantly reduced the cell growth rate (Figure 2G) and the number of the colonies by colony formation assay (Figure 2H), compared with those of the cells transfected with siRARS-001, siMAD1L1-002, or siCTL. These results suggest that endogenous RARS-MAD1L1 is required for the full growth and colony formation abilities of NPC cells *in vitro*.

### **RARS-MAD1L1 induces a SP of NPC cells**

It has been established that CSCs play an important role in tumor initiation and progression (22). To determine whether RARS-MAD1L1 has any effect on CSC properties, we examined the protein expression of CSC markers, including ATP-binding cassette (ABC) subfamily G member 2 (ABCG2), c-Myc, SRY-related HMG-box gene 2 (Sox2), and Bmi-1, by Western blotting. Our results showed that RARS-MAD1L1 overexpression upregulated the expression levels of these stem cell markers in CNE2 cells (Figure 3A) and S26 cells (Supplemental Figure 3A). ABCG2 has been implicated in multi-drug resistance. Therefore, we analyzed the cell-surface expression of ABCG2 by flow cytometry and immunofluorescence. A shift in ABCG2 staining intensity was observed in RARS-MAD1L1-expressing CNE2 cells and S26 cells compared with empty vector-containing control cells (21.1% vs. 3.1% in CNE2, 7.6% vs 1.1% in S26 cells, respectively) (Figure 3B and Supplemental Figure 3B). In addition to the increase in the immunostaining signal intensity for

ABCG2, RARS-MAD1L1 induced the localization of ABCG2 to the cell membrane (Figure 3C and Supplemental Figure 3C), where it performs its major function, leading to therapeutic resistance (23).

The presence of SP exhibiting CSC-like characteristics in NPC was previously reported (22). To investigate whether RARS-MAD1L1 induces the SP of NPC cells, we performed a flow cytometry analysis of Hoechst 33342-stained cells and found a clearly larger SP fraction among CNE2 cells overexpressing RARS-MAD1L1 ( $22.9\% \pm 4.253\%$ ) than among empty vector-harboring control cells ( $2.86\% \pm 0.5526\%$ ) (Figure 3D). Similarly, the SP ratio was also induced by RARS-MAD1L1 in S26 cells (Supplemental Figure 3D). Moreover, addition of the ABCG2 inhibitor FTC sufficiently reduced the incidence of Hoechst 33342-stained cells. We then performed a sphere-formation assay using empty vector- or RARS-MAD1L1-overexpressing CNE2 cells. As shown in Figure 3E, CNE2 cells expressing RARS-MAD1L1 cells formed more and larger spheres than CNE2 cells carrying the empty vector. These results suggest that *RARS-MAD1L1* might induce CSC-like characteristics.

### **RARS-MAD1L1 induces chemo- and radioresistance in NPC**

CSCs have been reported to play an important role in resistance to cancer therapy. As noted above, the ratio of the CSC-like SP was increased by RARS-MAD1L1. Therefore, we further investigated whether *RARS-MAD1L1* is

also involved in tumor resistance to radiotherapy and chemotherapy. DDP and 5-FU are the most common chemotherapeutic agents administered to advanced NPC patients. Thus, we used these drugs to evaluate drug sensitivity and found that the  $IC_{50}$  of RARS-MAD1L1-expressing CNE2 cells to DDP was increased to 1.68  $\mu\text{g/ml}$  compared with that of the vector-containing CNE2 cells (0.849  $\mu\text{g/ml}$ ) (Figure 3F). Moreover, the  $IC_{50}$  of RARS-MAD1L1-expressing CNE2 cells to 5-FU was increased to 0.520  $\mu\text{g}/\mu\text{l}$  compared with that of the vector-harboring cells (0.067  $\mu\text{g}/\mu\text{l}$ ) (Figure 3G). Furthermore, the RARS-MAD1L1-expressing CNE2 cells formed more colonies than the vector-carrying CNE2 cells under irradiation at 2 or 4 Gy (Figure 3H), suggesting that these cells have a more radioresistant phenotype that is likely conferred by the RARS-MAD1L1 fusion.

In addition, we examined the role of RARS-MAD1L1 in chemoresistance *in vivo*. We transplanted RARS-MAD1L1-expressing CNE2 cells or vector-harboring CNE2 cells into nude mice and treated the mice with DDP. As shown in Figure 3I, after DDP treatment, the mice transplanted with RARS-MAD1L1-expressing cells exhibited a shorter survival duration than the mice bearing the vector. After the mice were sacrificed, the vector-harboring CNE2 cell-based xenografts displayed a greater response to DDP than the RARS-MAD1L1-expressing cell-based xenografts (Figures 3J and 3K). These results suggest that RARS-MAD1L1 induced chemoresistance in cancer cells

*in vivo*. Taken together, these findings suggest that RARS-MAD1L1 induces resistance of NPC cells to both radiotherapy and chemotherapy, likely by enhancing CSC-like properties.

To eliminate the potential effects of HeLa contamination in the NPC cell lines (24, 25), we used the HK1 cell line for RARS-MAD1L1 overexpression and C666-1 cells for RARS-MAD1L1 knock-down experiments, and these cells were confirmed to be free of HeLa cell contamination (24, 25) (supplemental Table 2). RARS-MAD1L1 overexpression induced the expression of c-Myc and ABCG2 (Figure 4A), the cell-proliferation ability (Figure 4B) and the colony-formation ability (Figure 4C) in HK1 cells. Similarly, HK1 cells expressing RARS-MAD1L1 formed more colonies than HK1 cells with the vector under different doses of irradiation (Figure 4D). RARS-MAD1L1 expression in HK1 cells also enhanced cell survival upon different doses of chemotherapy [DDP (Figure 4E) and 5-FU (Figure 4F)]. These data further confirmed that RARS-MAD1L1 expression induced resistance to chemotherapy and radiotherapy.

### **RARS-MAD1L1 knockdown reduces CSC characteristics in NPC cells**

We sorted the SP and non-SP (NSP) fractions of the C666-1 cell population and analyzed *RARS-MAD1L1* expression by qPCR. Interestingly, *RARS-MAD1L1* expression was higher in the SP fraction of C666-1 cells than

in the NSP fraction (Supplemental Figure 4A). These results indicate that RARS-MAD1L1 might be associated with the SP of NPC cells. The knockdown of endogenous RARS-MAD1L1 decreased the expression of c-Myc and ABCG2 (Supplemental Figures 4B and 4C). The silencing of FUBP1 decreased the expression of c-Myc and ABCG2 (Supplemental Figure 5D) and the ratio of CD44+ cells (Supplemental Figure 4E) in C666-1 cells. In addition, treatment with the c-Myc inhibitor 10058-F4 reduced the expression of ABCG2 (Supplemental Figure 4F) and the ratio of CD44+ cells (Supplemental Figure 4G). These data further support the conclusion that RARS-MAD1L1 induces the expression of stem-cell markers and chemo-resistance in NPC cells, likely through the FUBP1/c-Myc axis. Because C666-1 does not form robust tumors in a xenograft tumor model *in vivo*, we did not perform these chemo-resistance experiments using C666-1 cells *in vivo*.

Because C666-1 is the only cell line that endogenously expresses RARS-MAD1L1, we conducted siRNA experiments in S26 cells overexpressing RARS-MAD1L1 (Supplemental Figure 5A). As shown in Supplemental Figure 6, the knockdown of RARS-MAD1L1 with two independent siRNAs (siRARS-005 and siMAD1L1-003) decreased cell proliferation (Supplemental Figure 5B) and the colony-formation ability (Supplemental Figure 5C) of S26 cells induced by RARS-MAD1L1 overexpression. Additionally, the silencing of RARS-MAD1L1 reduced the

radio-resistance (Supplemental Figure 5D) and chemo-resistance (Supplemental Figures 5E and 5F) of S26 cells induced by RARS-MAD1L1 overexpression. These results and the knockdown of endogenous RARS-MAD1L1 in C666-1 cells suggested the specificity of RARS-MAD1L1 siRNAs and that RARS-MAD1L1 induced radio-and chemo-resistance in NPC cells.

**RARS-MAD1L1 interacts with AIMP2 and increases the binding of Far upstream element (FUSE)-binding protein (FUBP1) to the c-Myc promoter**

To investigate the potential protein interactions of RARS-MAD1L1, we performed co-immunoprecipitation on CNE2 cells carrying the empty vector or expressing RARS-MAD1L1. As shown in Figure 5A, several potential RARS-MAD1L1 binding partners were isolated and visualized by silver staining. A subsequent mass spectrometry analysis showed that components of the aminoacyl-tRNA synthase (ARS) complex, including several t-RNA synthetases, AIMP1 and AIMP2, co-precipitated with RARS-MAD1L1.

In addition to serving as a scaffold for the multi-tRNA synthetase complex, AIMP2 is involved in various cancer biological pathways (26). AIMP2 has been shown to downregulate FUBP1, an upstream activator of c-Myc, resulting in reduced c-Myc activation (27). To further examine whether AIMP2 plays a role in mediating RARS-MAD1L1 functions, we first confirmed their interaction via

co-immunoprecipitation assays (Figure 5B). We subsequently investigated whether RARS-MAD1L1 expression has any effect on FUBP1. We conducted nuclear extraction assays and immunofluorescence to examine the levels of FUBP1 and performed ChIP assays to examine the interaction of FUBP1 with the c-Myc promoter. Although FUBP1 was only marginally upregulated in CNE2 RARS-MAD1L1 cells compared with CNE2 vector cells (Figures 5C and 5D), RARS-MAD1L1 induced significantly greater binding of FUBP1 to both the FUSE and P2 sites of the c-Myc promoter (Figure 5E). Taken together, these results show that RARS-MAD1L1 increased the expression of FUBP1 and the occupancy of the c-Myc promoter by FUBP1.

### **The oncogenic function of RARS-MAD1L1 is reduced by FUBP1 knockdown or treatment with a c-Myc inhibitor**

To further explore the role of FUBP1 in RARS-MAD1L1-mediated oncogenesis, we suppressed FUBP1 expression using two different siRNAs. We found that c-Myc and ABCG2 expression was reduced upon FUBP1 knock-down (Figures 6A and 6B). Transfection with a siRNA targeting FUBP1 alleviated the RARS-MAD1L1-induced enhancement of the colony-formation ability and the SP ratio in NPC cells (Figures 6C and 6D). These results indicate that the RARS-MAD1L1-mediated upregulation of FUBP1 might at least partially contribute to RARS-MAD1L1-induced tumor progression. Furthermore, we treated RARS-MAD1L1-expressing and vector-harboring stable CNE2 cell

lines with 10058-F4, which abrogates the interaction of c-Myc with Max and thus inhibits the activation of the downstream targets of c-Myc. Interestingly, treatment with 10058-F4 reduced the expression of ABCG2 and the SP ratio in RARS-MAD1L1-expressing CNE2 cells (Figures 6E and 6F). Similarly, knock-down of c-Myc reduced the expression of ABCG2 in RARS-MAD1L1-expressing CNE2 cells (Supplemental Figure 7). Using the MTT assay, we detected the survival of cells that overexpress RARS-MAD1L1 and were treated with the ABCG2 inhibitor ko143 and then with 5-FU. As shown in Figure 6G, ko143 markedly decreased the survival of RARS-MAD1L1-overexpressing CNE2 cells after treatment with 5-FU, suggesting that the inhibition of ABCG2 sensitized RARS-MAD1L1-overexpressing cells to chemotherapy. In addition, we detected the levels of ABCG2 and c-Myc to explore the correlation of RARS-MAD1L1 and these stem cell markers and found that the expression levels of ABCG2 and c-Myc in RARS-MAD1L1-positive patients were higher than those in the tumors that did not express RARS-MAD1L1 (Figures 6H-6I). These findings suggest that c-Myc is involved in the oncogenic function of RARS-MAD1L1. Taken together, our data suggest that the oncogenic function of RARS-MAD1L1 might be mediated, at least in part, via the FUBP1/c-Myc/ABCG2 axis.

## Discussion

In this study, we identified an in-frame *RARS-MAD1L1* fusion gene transcript in C666-1 cells by RNA-Seq and confirmed this aberration at the genomic level. We demonstrated that *RARS-MAD1L1* was a frequently observed fusion gene in NPC. Functionally, the silencing of endogenous *RARS-MAD1L1* repressed C666-1 cell proliferation and colony formation, whereas *RARS-MAD1L1* overexpression promoted the CSC-like properties of NPC cells by increasing the SP ratio and inducing chemoresistance and radioresistance. Furthermore, we demonstrated that the FUBP1/c-Myc axis was activated by *RARS-MAD1L1*. These findings might suggest that the development of drugs targeting this axis via combinatorial therapy could benefit NPC patients carrying this fusion gene.

Many fusion genes have been found in leukemia and lymphoma in past decades. However, in recent years, additional recurrent fusion genes have been discovered in solid tumors derived from epithelial tissues, and these fusion genes have been studied as diagnostic or prognostic markers. For example, the *TMPRSS2-ERG* fusion gene was identified in 33% of prostate cancer specimens collected via prostatectomy (28); *EML4-ALK* was detected in 6.7% of NSCLC specimens (14). *FGFR3-TACC3* was observed in 3.1% of glioblastoma specimens (29) and 2.5% of NPC specimens (16); *NAB2-STAT6* was found in 51% of solitary fibrous tumor specimens (30); and *UBR5-ZNF423* was identified in 8.3% of NPC specimens (17). In addition, most of these fusion genes are specific to a certain cancer type. *TMPRSS2-ERG* was only

observed in prostate cancer (13, 28), and *EML4-ALK* was only detected in NSCLC (14). However, *FGFR3-TACC3* was originally found in glioblastoma (29) and was subsequently also detected in NPC (16), head and neck cancer (16, 31), lung cancer (16, 31), bladder cancer (31) and other cancer types. Furthermore, we reported the presence of the *FGFR3-TACC3* fusion gene in approximately 2-4% of NPC, head and neck squamous cell carcinoma, esophageal squamous cell carcinoma and lung cancer samples (16). *FGFR3-TACC3* has been shown to induce oncogenic characteristics by activating FGFR kinase activity and is a potential therapeutic target (16, 18). *UBR5-ZNF423* was identified in the C666-1 NPC cell line and in 12/144 NPC tissues. Functional analysis suggests that *UBR5-ZNF423* might play an important role in tumorigenesis in a subset of NPC cases. This manuscript constitutes the first report of the detection of *RARS-MAD1L1* in other cancer types, including head and neck cancer. However, long-range PCR failed to determine the fusion point in DNA in the *RARS-MAD1L1*-positive tumor samples. The reasons are most likely due to the limit of the amplification length and ALU repeated sequence at the genomic DNA level or because only some of the tumor cells contained the fusion gene. In addition, because most of the NPC patients enrolled in this study were outpatients, detailed patient information was difficult to obtain. We have collected clinical information from 84 in-patient head and neck cancer samples and analyzed the correlation between *RARS-MAD1L1* and these parameters. Unfortunately,

RARS-MAD1L1 expression was not correlated with other clinical parameters, likely due to the limited sample size. Additionally, RARS-MAD1L1 was also present in 10.7% of the head and neck cancer cohort, indicating that RARS-MAD1L1 was not restricted to nasopharyngeal carcinoma but was also present in head and neck squamous cell carcinoma and parotid mucoepidermoid tumors. Whether the presence of RARS-MAD1L1 correlates with survival or metastasis and clinicopathological characteristics in a large cohort study of NPC patients or head and neck cancer patients must be further explored.

To date, few reports have indicated that fusion genes may cause the transformation of stem cells in malignancies, including leukemia (32, 33) and lung cancer (34). CSCs are a subset of tumor cells with self-renewal and proliferation abilities (35), and these cells play important roles in chemotherapy resistance, tumor recurrence and metastasis (36, 37). CSCs were originally identified in hematologic diseases (35) and were subsequently observed in many different types of cancer, such as brain (38), breast (39), and colon cancer (40). In addition, an SP of tumor cells exhibited stem-cell-like properties, and this population was identified in NPC and showed strong tumorigenesis ability and resistance to both chemotherapy and radiotherapy (22). Forced expression of MLL-ENL blocks cell differentiation (41), and the MLL-ENL-induced transformation of myeloid progenitors is mediated by the

upregulation of Hox genes (32, 42). Overexpression of MLL-AF9 in macrophage progenitors caused the transformation of these cells into leukemia stem cells (33). *CD47-NRG1*, which was discovered in invasive mucinous adenocarcinoma, induces CSC properties via the ErbB/PI3K/NF- $\kappa$ B pathway and the IGF2 autocrine/paracrine circuit (34). This manuscript provides the first evidence demonstrating that RARS-MAD1L1 upregulates CSC markers, increases the SP ratio, enhances sphere formation, and induces chemoresistance and radioresistance in NPC (Figures 3-4 and Supplemental Figure 4). Moreover, we found that the expression levels of c-Myc and ABCG2 in RARS-MAD1L1-positive patients were higher than those in the tumors that do not express RARS-MAD1L1 (Supplemental Figure 2B). This result suggests that RARS-MAD1L1 correlates with a high expression of stem cell markers, c-Myc and ABCG2, implying a role for RARS-MAD1L1 in enhancing CSC properties in NPC and head and neck cancer patients.

The C666-1 and HK1 cell lines were determined to be free of HeLa cell contamination. We observed similar results of RARS-MAD1L1 overexpression in CNE2 (Figure 2), HK1 (Figure 4) and S26 (Supplemental Figures 2 and 3) NPC cell lines. Similarly, the effects of RARS-MAD1L1 knockdown were comparable in both C666-1 cells (Supplemental Figure 4) and RARS-MAD1L1-overexpressing S26 cells (Supplemental Figure 5). These results suggest that the function of RARS-MAD1L1 could be a general

phenotype, which might not be strictly dependent on the cell type used.

*RARS*, as a fusion partner of *RARS-MAD1L1*, is one component of a complex composed of macromolecular ARSs and three ARS-interacting multi-functional proteins (AIMPs) that function in protein synthesis (43). In addition to assisting in the assembly of the ARS complex, AIMPs also play important roles in many other functions, including angiogenesis, tumorigenesis, and the DNA damage response (44). AIMP1 has antitumor potential by inhibiting angiogenesis and stimulating immunity (45). Both AIMP2 and AIMP3 are released from the ARS complex upon DNA damage. AIMP3 acts as a potent tumor suppressor gene by upregulating p53 in response to DNA damage (46). AIMP2 can interact with p53 and decrease p53 degradation, leading to increased susceptibility to DNA damage (47). AIMP2 might also facilitate the degradation of certain proteins. For instance, upon TNF- $\alpha$  treatment, AIMP2 can increase the ubiquitination of TRAF2, leading to cell apoptosis and a further reduction in NF- $\kappa$ B activity (48). In addition, induction of AIMP2 by TGF- $\beta$  promotes FUBP1 degradation (27). In the current study, we found that *RARS-MAD1L1* interacts with AIMP2 and other components of the ARS complex (Figure 4), likely leading to suppression of the release of AIMP2 from the ARS complex. Thus, we measured the expression of the targets of AIMP2 and found that FUBP1 was upregulated (Figure 4) but that the p53 and NF- $\kappa$ B levels were unchanged in *RARS-MAD1L1*-expressing cells

(data not shown). Taken together, our data indicate that the interaction between RARS-MAD1L and AIMP2 might suppress the release of AIMP2 and increase FUBP1 expression, likely due to a reduction in FUBP1 degradation.

Because part of the 270-a.a. RARS constitutes most of the RARS-MAD1L1 protein, we also established a RARS-overexpressing stable CNE2 cell line (Supplemental Figure 6A) to compare the effects of wild-type RARS and RARS-MAD1L1. As shown in Supplemental Figure 6B, 6C and 6D, RARS overexpression induced the expression of ABCG2 and the cell proliferation ability and SP ratio in CNE2 cells but to a lesser extent compared with the effects of RARS-MAD1L1, suggesting that RARS-MAD1L1 has a stronger oncogenic function than RARS alone. In addition, the mRNA of RARS was less stable in CNE2-RARS-MAD1L1 than that in CNE2-vector cells whereas the mRNA stability of MAD1L1 was not changed upon overexpression of RARS-MAD1L1 (Supplemental Figure 6E). This data indicated that RARS-MAD1L1 might influence the stability of RARS to act its oncogenic function. Although RARS-MAD1L1 has indeed the similar function of RARS, this fusion gene might influence the expression of RARS to act its strong oncogenic function.

CSCs are known to contribute to the resistance of cancer to irradiation and chemotherapy (22). FUBP1 was identified based on its binding to the FUSE of

the c-Myc promoter and was thus found to stimulate c-Myc expression (49). Our previous study showed that FUBP1 is a prognostic biomarker for NPC and that FUBP1 expression correlates with c-Myc expression. FUBP1 induces c-Myc expression and promotes CSC-like properties in NPC (50). In this study, we found that the RARS-MAD1L1 fusion protein increased FUBP1 expression, contributing to increased occupancy of the c-Myc promoter by FUBP1 (Figure 5), the upregulation of c-Myc, and the induction of CSC-like properties (Figure 3 and 4). The knockdown of FUBP1 and treatment with a c-Myc inhibitor decreased the expression of ABCG2, a direct downstream target of c-Myc, and the SP ratio of NPC cells expressing RARS-MAD1L1 (Figure 6). c-Myc is a key regulator for the maintenance of CSC properties (51). c-Myc can induce radioresistance via CHK1 and CHK2 (52) and chemoresistance via upregulation of the ABC transporter family of genes, including ABCG2 (53). ABCG2 plays an important role in the chemoresistance of CSCs by facilitating drug efflux (54). In our study, we showed that RARS-MAD1L1-expressing CNE2 cells have stronger radioresistant and chemoresistant abilities than control cells (Figure 3 and 4). In addition, RARS-MAD1L1 overexpression upregulates c-Myc and ABCG2 and induces the distribution of ABCG2 on the cell membrane (Figure 3). A Myc inhibitor abrogates the induction of ABCG2 expression and SP expansion by RARS-MAD1L1 (Figure 6). Taken together, our data suggest that the CSC-like characteristics induced by RARS-MAD1L1 might result from induction of the FUBP1/c-Myc axis.

*MAD1L1*, the mitosis checkpoint gene and other fusion partner within RARS-*MAD1L1*, consists of 660 a.a. and contains an N-terminal coil-coil domain and a conserved C-terminal domain (CTD) (595-718 amino acids) that plays a role in kinetochore targeting (55). *MAD1L1* was shown to interact with *MAD2* to form a mitotic spindle-assembly checkpoint core complex and to convert *MAD2* from its open form to its closed form (19, 56). These events prevent the onset of anaphase until all chromosomes are properly aligned at the metaphase plate, thereby avoiding aneuploidy and chromosomal instability (57). The RARS-*MAD1L1* fusion protein was composed of 273 a.a. of the RARS protein and 51 a.a. of the *MAD1L1* protein. In our study, we found that RARS-*MAD1L1* did not interact with *MAD2* (data not shown), and neither micronucleus formation nor aneuploidy was apparent in RARS-*MAD1L1*-expressing cells (data not shown). This observation suggests that RARS-*MAD1L1* might not function via *MAD1L1*.

In summary, we demonstrated the presence of the recurrent *RARS-MAD1L1* gene fusion in NPC. Furthermore, we provided the first evidence showing that the RARS-*MAD1L1* fusion gene enhances tumorigenicity, CSC-like properties, and therapeutic resistance, at least in part, via the FUBP1/c-Myc axis (Supplemental Figure 8). These findings might implicate RARS-*MAD1L1* as an attractive target for therapeutic intervention in NPC.

**Competing Financial Interests Statement:** VWY served as a scientific consultant for Novartis Pharmaceuticals (HK) Limited. The authors have no relevant conflicts of interest. The authors declare no competing financial interests.

### **Author Contributions:**

Conception and design: X. Zhang and M.S. Zeng

Development of methodology: Q. Zhong, Z.H. Liu, Z.R. Lin<sup>1</sup>, Z.D. Hu, L. Yuan, L.H. Xu,  
L.J. Hu, and Z.F. Wang

Acquisition of data (provided animals, acquired and managed patients,  
provided facilities, etc.): Q. Zhong, Z.H. Liu, Z.R. Lin<sup>1</sup>, Z.D. Hu, L. Yuan, Y.M. Liu, A. J.  
Zhou, L.H. Xu and L.J. Hu

Analysis and interpretation of data (e.g., statistical analysis, biostatistics,  
computational analysis): Q. Zhong, Z.H. Liu, Z.R. Lin<sup>1</sup>, Z.D. Hu and Y.M. Liu,

Writing, review, and/or revision of the manuscript: Q. Zhong and Z.H. Liu

Administrative, technical, or material support (i.e., reporting or organizing data,  
constructing databases): X.Y. Guan, J.J. Hao, V.W.Y. Lui, L. Guo, H.Q. Mai, M.Y. Chen,  
F. Han, Y.F.Xia and J.R. Grandis

Study supervision: Q. Zhong and M.S. Zeng

## **Acknowledgments**

This work was supported by the grants from National Key R&D Program of China (2017YFA0505600-04, MSZ), the Ministry of Science and Technology of China (2013CB910500 and 2015AA020931) (ZX and ZQ), the National Natural Science Foundation of China (81230045, 91440106, 81161120408, 81572600, 81772883, and 81520108022) (MSZ and ZQ), the Science and Technology project of Guangdong Province (2014B050504004, 2015B050501005, MSZ), the talent program of Guangdong Province (412022693047, ZQ), the National Cancer Institute Head and Neck Cancer SPORE P50 CA097190 (JRG), the School of Biomedical Sciences Start-up Fund, the Chinese University of Hong Kong (VWYL), the General Research Fund (#17114814) (VWYL) and the Theme-based Research Scheme (T12-401/13-R), Research Grant Council, Hong Kong (VWYL). The funders had no role in study design, data collection and analysis, the decision to publish, or the preparation of the manuscript. The authenticity of this article has been validated by uploading the key raw data onto the Research Data Deposit public platform ([www.researchdata.org.cn](http://www.researchdata.org.cn)), with the approval number RDDB2017000 123.

## References

1. Zhang LF, Li YH, Xie SH, Ling W, Chen SH, Liu Q, et al. Incidence trend of nasopharyngeal carcinoma from 1987 to 2011 in Sihui County, Guangdong Province, South China: an age-period-cohort analysis. *Chinese journal of cancer*. 2015;34:350-7.
2. Wei KR, Zheng RS, Zhang SW, Liang ZH, Ou ZX, Chen WQ. Nasopharyngeal carcinoma incidence and mortality in China in 2010. *Chinese journal of cancer*. 2014;33:381-7.
3. Chen MY, Jiang R, Guo L, Zou X, Liu Q, Sun R, et al. Locoregional radiotherapy in patients with distant metastases of nasopharyngeal carcinoma at diagnosis. *Chinese journal of cancer*. 2013;32:604-13.
4. Loong HH, Ma BB, Chan AT. Update on the management and therapeutic monitoring of advanced nasopharyngeal cancer. *Hematology/oncology clinics of North America*. 2008;22:1267-78, x.
5. Hanahan D, Weinberg RA. Hallmarks of cancer: the next generation. *Cell*. 2011;144:646-74.
6. Hui AB, Lo KW, Leung SF, Teo P, Fung MK, To KF, et al. Detection of recurrent chromosomal gains and losses in primary nasopharyngeal carcinoma by comparative genomic hybridisation. *International journal of cancer*. 1999;82:498-503.
7. Hui AB, Lo KW, Leung SF, Choi PH, Fong Y, Lee JC, et al. Loss of heterozygosity on the long arm of chromosome 11 in nasopharyngeal

carcinoma. *Cancer research*. 1996;56:3225-9.

8. Huang DP, Lo KW, Choi PH, Ng AY, Tsao SY, Yiu GK, et al. Loss of heterozygosity on the short arm of chromosome 3 in nasopharyngeal carcinoma. *Cancer genetics and cytogenetics*. 1991;54:91-9.

9. Or YY, Hui AB, Tam KY, Huang DP, Lo KW. Characterization of chromosome 3q and 12q amplicons in nasopharyngeal carcinoma cell lines. *International journal of oncology*. 2005;26:49-56.

10. Bunting SF, Nussenzweig A. End-joining, translocations and cancer. *Nature reviews Cancer*. 2013;13:443-54.

11. Heisterkamp N, Stam K, Groffen J, de Klein A, Grosveld G. Structural organization of the bcr gene and its role in the Ph' translocation. *Nature*. 1985;315:758-61.

12. O'Brien SG, Guilhot F, Larson RA, Gathmann I, Baccarani M, Cervantes F, et al. Imatinib compared with interferon and low-dose cytarabine for newly diagnosed chronic-phase chronic myeloid leukemia. *The New England journal of medicine*. 2003;348:994-1004.

13. Tomlins SA, Rhodes DR, Perner S, Dhanasekaran SM, Mehra R, Sun XW, et al. Recurrent fusion of TMPRSS2 and ETS transcription factor genes in prostate cancer. *Science*. 2005;310:644-8.

14. Soda M, Choi YL, Enomoto M, Takada S, Yamashita Y, Ishikawa S, et al. Identification of the transforming EML4-ALK fusion gene in non-small-cell lung cancer. *Nature*. 2007;448:561-6.

15. Shaw AT, Kim DW, Nakagawa K, Seto T, Crino L, Ahn MJ, et al. Crizotinib versus chemotherapy in advanced ALK-positive lung cancer. *The New England journal of medicine*. 2013;368:2385-94.
16. Yuan L, Liu ZH, Lin ZR, Xu LH, Zhong Q, Zeng MS. Recurrent FGFR3-TACC3 fusion gene in nasopharyngeal carcinoma. *Cancer biology & therapy*. 2014;15:1613-21.
17. Chung GT, Lung RW, Hui AB, Yip KY, Woo JK, Chow C, et al. Identification of a recurrent transforming UBR5-ZNF423 fusion gene in EBV-associated nasopharyngeal carcinoma. *The Journal of pathology*. 2013;231:158-67.
18. Capelletti M, Dodge ME, Ercan D, Hammerman PS, Park SI, Kim J, et al. Identification of recurrent FGFR3-TACC3 fusion oncogenes from lung adenocarcinoma. *Clin Cancer Res*.20:6551-8.
19. Luo X, Tang Z, Rizo J, Yu H. The Mad2 spindle checkpoint protein undergoes similar major conformational changes upon binding to either Mad1 or Cdc20. *Molecular cell*. 2002;9:59-71.
20. Li YH, Wang F, Shen L, Deng YM, Shao Q, Feng F, et al. EGFR fluorescence in situ hybridization pattern of chromosome 7 disomy predicts resistance to cetuximab in KRAS wild-type metastatic colorectal cancer patients. *Clinical cancer research : an official journal of the American Association for Cancer Research*. 2011;17:382-90.
21. Li Y, Chen L, Nie CJ, Zeng TT, Liu H, Mao X, et al. Downregulation of RBMS3 is associated with poor prognosis in esophageal squamous cell

carcinoma. *Cancer research*. 2011;71:6106-15.

22. Wang J, Guo LP, Chen LZ, Zeng YX, Lu SH. Identification of cancer stem cell-like side population cells in human nasopharyngeal carcinoma cell line. *Cancer research*. 2007;67:3716-24.

23. Bleau AM, Hambardzumyan D, Ozawa T, Fomchenko EI, Huse JT, Brennan CW, et al. PTEN/PI3K/Akt pathway regulates the side population phenotype and ABCG2 activity in glioma tumor stem-like cells. *Cell stem cell*. 2009;4:226-35.

24. Strong MJ, Baddoo M, Nanbo A, Xu M, Puetter A, Lin Z. Comprehensive high-throughput RNA sequencing analysis reveals contamination of multiple nasopharyngeal carcinoma cell lines with HeLa cell genomes. *Journal of virology*. 2014;88:10696-704.

25. Chan SY, Choy KW, Tsao SW, Tao Q, Tang T, Chung GT, et al. Authentication of nasopharyngeal carcinoma tumor lines. *International journal of cancer*. 2008;122:2169-71.

26. Guo M, Schimmel P. Essential nontranslational functions of tRNA synthetases. *Nature chemical biology*. 2013;9:145-53.

27. Kim MJ, Park BJ, Kang YS, Kim HJ, Park JH, Kang JW, et al. Downregulation of FUSE-binding protein and c-myc by tRNA synthetase cofactor p38 is required for lung cell differentiation. *Nature genetics*. 2003;34:330-6.

28. Saramaki OR, Harjula AE, Martikainen PM, Vessella RL, Tammela TL,

Visakorpi T. TMPRSS2:ERG fusion identifies a subgroup of prostate cancers with a favorable prognosis. *Clinical cancer research : an official journal of the American Association for Cancer Research*. 2008;14:3395-400.

29. Singh D, Chan JM, Zoppoli P, Niola F, Sullivan R, Castano A, et al. Transforming fusions of FGFR and TACC genes in human glioblastoma. *Science*. 2012;337:1231-5.

30. Robinson DR, Wu YM, Kalyana-Sundaram S, Cao X, Lonigro RJ, Sung YS, et al. Identification of recurrent NAB2-STAT6 gene fusions in solitary fibrous tumor by integrative sequencing. *Nature genetics*. 2013;45:180-5.

31. Wu YM, Su F, Kalyana-Sundaram S, Khazanov N, Ateeq B, Cao X, et al. Identification of targetable FGFR gene fusions in diverse cancers. *Cancer discovery*. 2013;3:636-47.

32. So CW, Karsunky H, Passegue E, Cozzio A, Weissman IL, Cleary ML. MLL-GAS7 transforms multipotent hematopoietic progenitors and induces mixed lineage leukemias in mice. *Cancer cell*. 2003;3:161-71.

33. Krivtsov AV, Twomey D, Feng Z, Stubbs MC, Wang Y, Faber J, et al. Transformation from committed progenitor to leukaemia stem cell initiated by MLL-AF9. *Nature*. 2006;442:818-22.

34. Murayama T, Nakaoku T, Enari M, Nishimura T, Tominaga K, Nakata A, et al. Oncogenic Fusion Gene CD74-NRG1 Confers Cancer Stem Cell-like Properties in Lung Cancer through a IGF2 Autocrine/Paracrine Circuit. *Cancer research*. 2016;76:974-83.

35. Park CH, Bergsagel DE, McCulloch EA. Mouse myeloma tumor stem cells: a primary cell culture assay. *Journal of the National Cancer Institute*. 1971;46:411-22.
36. Reya T, Morrison SJ, Clarke MF, Weissman IL. Stem cells, cancer, and cancer stem cells. *Nature*. 2001;414:105-11.
37. Dick JE. Looking ahead in cancer stem cell research. *Nature biotechnology*. 2009;27:44-6.
38. Singh SK, Clarke ID, Terasaki M, Bonn VE, Hawkins C, Squire J, et al. Identification of a cancer stem cell in human brain tumors. *Cancer research*. 2003;63:5821-8.
39. Al-Hajj M, Wicha MS, Benito-Hernandez A, Morrison SJ, Clarke MF. Prospective identification of tumorigenic breast cancer cells. *Proceedings of the National Academy of Sciences of the United States of America*. 2003;100:3983-8.
40. O'Brien CA, Pollett A, Gallinger S, Dick JE. A human colon cancer cell capable of initiating tumour growth in immunodeficient mice. *Nature*. 2007;445:106-10.
41. Zeisig BB, Garcia-Cuellar MP, Winkler TH, Slany RK. The oncoprotein MLL-ENL disturbs hematopoietic lineage determination and transforms a biphenotypic lymphoid/myeloid cell. *Oncogene*. 2003;22:1629-37.
42. Cozzio A, Passegue E, Ayton PM, Karsunky H, Cleary ML, Weissman IL. Similar MLL-associated leukemias arising from self-renewing stem cells and

short-lived myeloid progenitors. *Genes & development*. 2003;17:3029-35.

43. Ling C, Yao YN, Zheng YG, Wei H, Wang L, Wu XF, et al. The C-terminal appended domain of human cytosolic leucyl-tRNA synthetase is indispensable in its interaction with arginyl-tRNA synthetase in the multi-tRNA synthetase complex. *The Journal of biological chemistry*. 2005;280:34755-63.

44. Park SG, Ewalt KL, Kim S. Functional expansion of aminoacyl-tRNA synthetases and their interacting factors: new perspectives on housekeepers. *Trends in biochemical sciences*. 2005;30:569-74.

45. Han JM, Myung H, Kim S. Antitumor activity and pharmacokinetic properties of ARS-interacting multi-functional protein 1 (AIMP1/p43). *Cancer letters*. 2010;287:157-64.

46. Park BJ, Oh YS, Park SY, Choi SJ, Rudolph C, Schlegelberger B, et al. AIMP3 haploinsufficiency disrupts oncogene-induced p53 activation and genomic stability. *Cancer research*. 2006;66:6913-8.

47. Han JM, Park BJ, Park SG, Oh YS, Choi SJ, Lee SW, et al. AIMP2/p38, the scaffold for the multi-tRNA synthetase complex, responds to genotoxic stresses via p53. *Proceedings of the National Academy of Sciences of the United States of America*. 2008;105:11206-11.

48. Choi JW, Kim DG, Park MC, Um JY, Han JM, Park SG, et al. AIMP2 promotes TNFalpha-dependent apoptosis via ubiquitin-mediated degradation of TRAF2. *Journal of cell science*. 2009;122:2710-5.

49. Duncan R, Bazar L, Michelotti G, Tomonaga T, Krutzsch H, Avigan M, et al.

A sequence-specific, single-strand binding protein activates the far upstream element of c-myc and defines a new DNA-binding motif. *Genes & development*. 1994;8:465-80.

50. Liu ZH, Hu JL, Liang JZ, Zhou AJ, Li MZ, Yan SM, et al. Far upstream element-binding protein 1 is a prognostic biomarker and promotes nasopharyngeal carcinoma progression. *Cell death & disease*. 2015;6:e1920.

51. Kim J, Woo AJ, Chu J, Snow JW, Fujiwara Y, Kim CG, et al. A Myc network accounts for similarities between embryonic stem and cancer cell transcription programs. *Cell*. 2010;143:313-24.

52. Wang WJ, Wu SP, Liu JB, Shi YS, Huang X, Zhang QB, et al. MYC regulation of CHK1 and CHK2 promotes radioresistance in a stem cell-like population of nasopharyngeal carcinoma cells. *Cancer research*. 2013;73:1219-31.

53. Porro A, Haber M, Diolaiti D, Iraci N, Henderson M, Gherardi S, et al. Direct and coordinate regulation of ATP-binding cassette transporter genes by Myc factors generates specific transcription signatures that significantly affect the chemoresistance phenotype of cancer cells. *The Journal of biological chemistry*. 2010;285:19532-43.

54. An Y, Ongkeko WM. ABCG2: the key to chemoresistance in cancer stem cells? *Expert opinion on drug metabolism & toxicology*. 2009;5:1529-42.

55. Maldonado M, Kapoor TM. Constitutive Mad1 targeting to kinetochores uncouples checkpoint signalling from chromosome biorientation. *Nature cell*

biology. 2011;13:475-82.

56. Sironi L, Mapelli M, Knapp S, De Antoni A, Jeang KT, Musacchio A. Crystal structure of the tetrameric Mad1-Mad2 core complex: implications of a 'safety belt' binding mechanism for the spindle checkpoint. *The EMBO journal*. 2002;21:2496-506.

57. Jin DY, Kozak CA, Pangilinan F, Spencer F, Green ED, Jeang KT. Mitotic checkpoint locus MAD1L1 maps to human chromosome 7p22 and mouse chromosome 5. *Genomics*. 1999;55:363-4.

## Figure legends

### Figure 1. Characterization of the RARS-MAD1L1 genomic rearrangement in C666-1 cells.

A. The schematic diagrams in the top panel show the genomic location of the RARS and MAD1L1 genes. B. FISH assays were performed to validate the presence of the RARS-MAD1L1 fusion gene in C666-1 cells using two paired sets of probes (NONSC35A9 and NONSC15B2; RP11-318C9 and RP11-510K8) (red, RARS; green, MAD1L1). The white arrow denotes the merged yellow positive signal. Lymphocytes were used as negative controls. C. Genomic rearrangement forming the RARS-MAD1L1 fusion gene in C666-1 cells (red: RARS, green: MAD1L1; black, an insertion of a portion of HDAC9). D. Schematic graph of the predicted fusion protein. E. Detection of the endogenous expression of the RARS-MAD1L1 fusion gene in C666-1 cells using an N-terminal RARS antibody. HeLa cells transiently transfected with pBabe-RARS-MAD1L1 and CNE2 cells were used as positive and negative controls, respectively. F. Detection of RARS-MAD1L1 endogenous protein by immunoprecipitation with a C-terminal MAD1L1 antibody and probing with an N-terminal RARS antibody. Rabbit IgG served as a negative control. 293FT cells transfected with RARS-MAD1L1 were used as a positive control. The black arrow denotes the band corresponding to RARS-MAD1L1. G. Reverse-transcription-PCR detection of a specific 891-bp fragment in RARS-MAD1L1 fusion gene-positive tumor RNA (01) but not in negative tumor

RNA (02). C666-1 and H<sub>2</sub>O served as the positive (+) and negative (-) controls, respectively. M, 100-bp ladder. The sequencing results (lower panel) and scheme (upper panel) of the PCR product of RARS-MAD1L1 are shown. The black dash annotates the breakpoint of genomic DNA from positive tumor RNA. H. FISH assays were performed to validate the presence of the RARS-MAD1L1 fusion gene in interphase nuclei of fresh NPC tissues using one paired set of probes (NONSC35A9 and NONSC15B2). Lymphocytes were used as negative controls. I. FISH assays were performed to validate the presence of the RARS-MAD1L1 fusion gene in FFPE NPC tissues using two paired sets of probes (NONSC35A9 and NONSC15B2; RP11-318C9 and RP11-510K8). The white arrow denotes the merged yellow positive signal.

**Figure 2. Oncogenic potential of the RARS-MAD1L1 fusion gene.**

A. Representative Western blotting images of CNE2 cells stably expressing RARS-MAD1L1 or pBabe (empty vector). B. Growth curves of CNE2 cells stably expressing RARS-MAD1L1 or pBabe (vector). The growth was determined through the MTT assay; n=5 wells per group; \* refers to differences between RARS-MADL1 and pBabe (vector) ( $p < 0.05$ , as determined by two-way ANOVA). C-D. Colony-formation assays (C) and anchorage-independent growth assays (D) (at magnifications of 40X and 100X) of CNE2 cells stably expressing RARS-MAD1L1 or pBabe (vector). The results of quantitative analysis of these assays are shown adjacent to the images. The

experiments were repeated three times; n=9; \* refers to differences between RARS-MAD1L1 and pBabe (vector) (\*\*\*, p<0.001, as determined by Student's t-test). E. qPCR analysis of RARS, MAD1L1, and RARS-MAD1L1 expression in C666-1 cells after transfection with siRARS-001, siRARS-005, siMAD1L1-002, siMAD1L1-003, or scramble siRNA (siCTL). F. Representative Western blotting images of C666-1 cells transfected with siRARS-001, siRARS-005, siMAD1L1-002, siMAD1L1-003, or scramble siRNA (siCTL). G. CCK8 assays of C666-1 cells seeded 24 h after transfection with siRNA and then cultured for the indicated period; n=5 wells per group; \* refers to differences between siCTL and siRARS-005 or siMAD1L1-003 (\*, p<0.05, \*\*, p<0.01, and \*\*\*, p<0.001, as determined by two-way analysis of variance (ANOVA) followed by the Bonferroni post-hoc test). H. Colony-formation assays of C666-1 cells seeded 24 h after transfection with siRNA as indicated and then cultured for 10 days.

### **Figure 3. RARS-MAD1L1 enhances CSC properties in CNE2 cells.**

A. Representative Western blotting images of ABCG2, c-Myc, BMI-1, and Sox2 expression in CNE2 cells stably expressing RARS-MAD1L1 or pBabe (vector).  
B. Flow cytometry analysis of ABCG2-enriched CNE2 cells. C. Immunofluorescence images of CNE2 cells stained for ABCG2 (green) and WGA (red). Nuclei were stained with DAPI (blue). Original magnification, 600X.  
D. Flow cytometry analysis of Hoechst 33342 staining was performed on

CNE2 cells stably expressing RARS-MAD1L1 or pBabe (vector) (upper panel). FTC at a final concentration of 5  $\mu$ M was added before Hoechst 33342 staining (lower panel). The percentage of cells in the SP is presented. E. Representative phase images of sphere formation by stable CNE2 cells (magnification, 100X). The numbers of spheres formed by these cells are shown in the right panel. F-G. Growth curves of CNE2 cells stably expressing RARS-MAD1L1 or pBabe (vector) 48 h post-treatment with the indicated dose of DDP (F) or 5-FU (G). H. Representative images of CNE2 cells stably expressing RARS-MAD1L1 or pBabe (vector) cultured for 10 days after X-irradiation with the indicated dose (Gy). I-K. Survival curve (I), tumor images (J), and growth curve (K) of nude mice inoculated with CNE2 cells stably expressing RARS-MAD1L1 or pBabe (vector) and intraperitoneally injected with DDP. In I, n=14 mice per group for vector and RARS-MAD1L1. In J and K, n=7 mice per group for vector-vehicle, vector-DDP RARS-MAD1L1-vehicle and RARS-MAD1L1-DDP. In D and E, n=9, and in G, n=5; \* refers to differences between RARS-MAD1L1 and pBabe (vector) (\*\*,  $p < 0.01$ , as determined by Student's t-test). In I, n=14, and K, n=7; \* refers to differences between RARS-MAD1L1-DDP and pBabe (vector)-DDP (\*,  $p < 0.05$ , \*\*\*,  $p < 0.001$ , as determined by a log-rank test (I) or one way analysis of variance (ANOVA) followed by the Bonferroni post-hoc test (K)).

**Figure 4. RARS-MAD1L1 promotes proliferation and CSC-like properties**

**in HK1 cells.**

A. Representative Western blotting images of HK1 stably expressing RARS-MAD1L1 or pBabe (vector). B. Growth curves of HK1 stably expressing RARS-MAD1L1 or pBabe (vector). Growth was determined through the MTT assay, n=5 wells per group; C. Colony-formation assay and quantitative analysis of HK1 stably expressing RARS-MAD1L1 or pBabe (vector). The experiments were repeated three times; n=3; (\*, p<0.05, as determined by Student's t-test). D. Representative images of CNE2 cells stably expressing RARS-MAD1L1 or pBabe (vector) cultured for 10 days after X-irradiation with the indicated Gy dose. E-F. Growth curves of CNE2 cells stably expressing RARS-MAD1L1 or pBabe (vector) 48 h post-treatment with the indicated dose of DDP (E) or 5-FU (F). \* refers to differences between RARS-MAD1L1 and pBabe (vector). For B, E, and F, n=5 wells per group (\*, p<0.05, \*\*, p<0.01, \*\*\*, p<0.001 as determined by two-way analysis of variance (ANOVA) followed by the Bonferroni post-hoc test).

**Figure 5. RARS-MAD1L1 interacts with AIMP2 and increases the binding of FUBP1 to the c-Myc promoter.**

A. Detection of RARS-MAD1L1-interacting proteins via immunoprecipitation with an anti-Flag antibody followed by silver staining of CNE2 cells stably expressing RARS-MAD1L1 or pBabe (vector). B. Detection of the interaction of RARS-MAD1L1 with AIMP2 via immunoprecipitation with an anti-Flag antibody

or AIMP2 antibody and probing with an antibody against AIMP2 or Flag in CNE2 cells stably expressing RARS-MAD1L1 or pBabe (vector). The input served as a positive control. C. Representative Western blotting images of FUBP1, lamin B1 and GAPDH protein expression in the cytoplasm and nuclear extract (NE) fractions from CNE2 cells stably expressing RARS-MAD1L1 or pBabe (vector). D. Immunofluorescence images of FUBP1 (red) staining in CNE2 cells stably expressing RARS-MAD1L1 or pBabe. Nuclei were stained with DAPI (blue). Original magnification: 600X. E. RARS-MAD1L1 enhances the occupancy of the Fuse and P2 sites of the c-Myc promoter by FUBP1. ChIP assays were performed using an antibody against FUBP1 in CNE2 cells stably expressing RARS-MAD1L1 or pBabe (vector), and qPCR was used to quantify the levels of amplified DNA. Rabbit IgG served as a negative control; n=9; \* refers to differences between RARS-MAD1L1 and pBabe (vector) (\*\*\*, p<0.001, as determined by two-way ANOVA followed by the Bonferroni post-hoc test).

**Figure 6. The oncogenic activity of RARS-MAD1L1 is suppressed by FUBP1 knockdown or treatment with a c-Myc inhibitor.**

A. qPCR analysis of FUBP1, c-Myc, and ABCG2 expression in CNE2 cells stably expressing RARS-MAD1L1 or pBabe (vector) after transfection with siRNA-FUBP1#1 (siFUBP1-#1), siRNA-FUBP1#2 (siFUBP1-#2) or siCTL. B. Representative Western blotting images of FUBP1, c-Myc, ABCG2, and Flag

expression in CNE2 cells stably expressing RARS-MAD1L1 or pBabe (vector) after transfection with siFUBP1-#1, siFUBP1-#2 or siCTL.  $\beta$ -actin served as a negative control. C. Representative images and quantitative analysis of colony formation by CNE2 cells stably expressing RARS-MAD1L1 or pBabe (vector) seeded 24 h after transfection with siRNA and then cultured for seven days. D. Flow cytometry analysis of Hoechst 33342-stained CNE2 cells stably expressing RARS-MAD1L1 or pBabe (vector) after transfection with siFUBP1-#1, siFUBP1-#2 or siCTL. The percentage of cells in the SP is indicated. E. qPCR analysis and Western blotting of ABCG2 expression in CNE2 cells stably expressing RARS-MAD1L1 or pBabe (vector) after treatment with 10058-F4 or DMSO. F. Flow cytometry analysis of Hoechst 33342-stained CNE2 cells stably expressing RARS-MAD1L1 or pBabe (vector) after treatment with 10058-F4 or DMSO. G. Cell survival rate of CNE2 cells stably expressing RARS-MAD1L1 or pBabe (vector) pretreated with ko143 or DMSO for 2 h and then treated with 5-FU in the presence of ko143 or DMSO for 48 h. H-I. The relative expression levels of ABCG2 (H) and c-MYC (I) were detected in RARS-MAD1L1-positive and RARS-MAD1L1-negative HNC patients. The percentage of cells in the SP is presented. In A, C, and D, n=9; \* refers to differences between siCTL and siFUBP1#1, or siFUBP1#2 (\*, p<0.05, \*\*, p<0.01). In F, n=9; \* refers to differences between DMSO and 10058-F4 treatment (\*\*\*, p<0.001). In G, n=5; \* refers to differences between DMSO and ko143 treatment (\*\*\*, p<0.001). Significance was calculated by two-way

analysis of variance (ANOVA) followed by the Bonferroni post-hoc test. In H and I, \* refers to differences between RARS-MAD1L1-positive HNC patients (n=54) and RARS-MAD1L1-negative HNC patients (n=9) (\*,  $p < 0.05$ ).

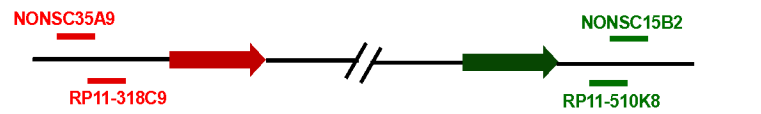
Significance was calculated by unpaired t-test.

Figure 1

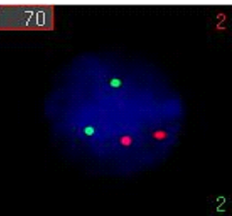
A



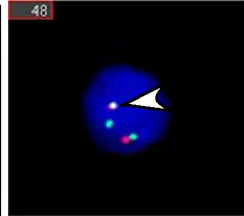
B



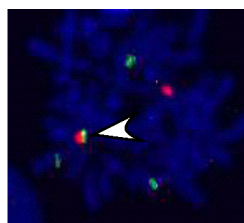
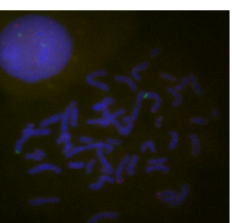
normal peripheral blood cells



C666-1 cells

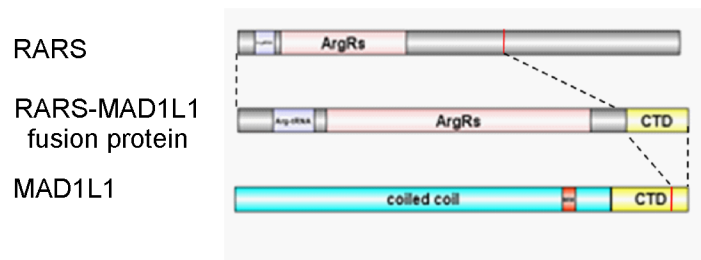


RARS:NONSC 35A9  
MAD1L1:NONSC15B2

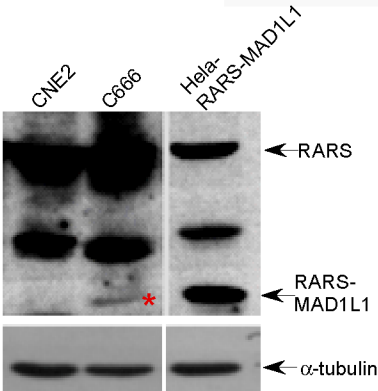


RARS:RP11-318C9  
MAD1L1:RP11-510K8

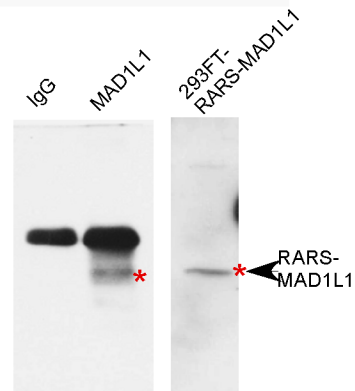
D



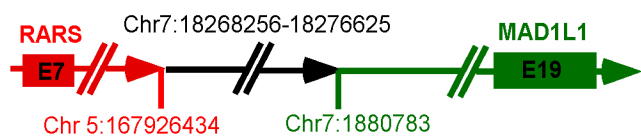
E



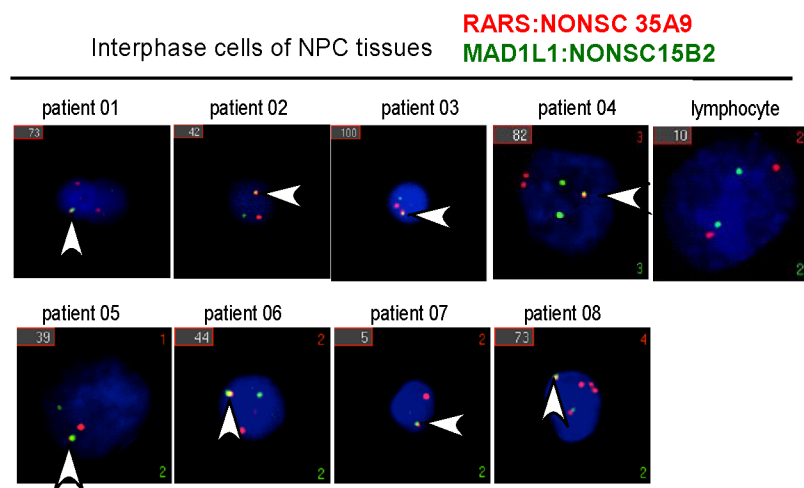
F



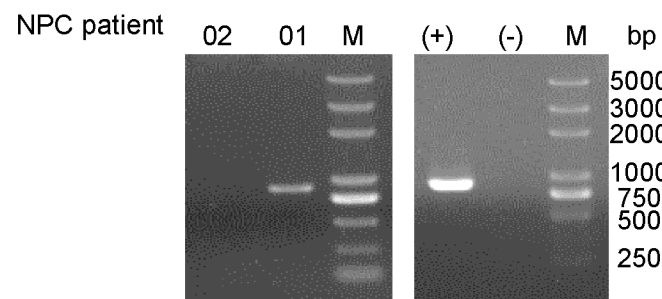
C



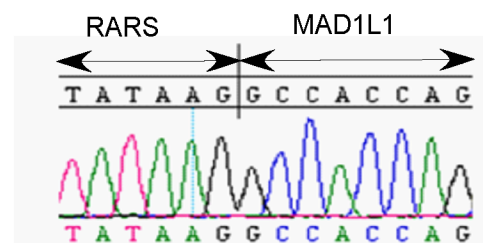
H



G



RARS-MAD1L1 cDNA



I

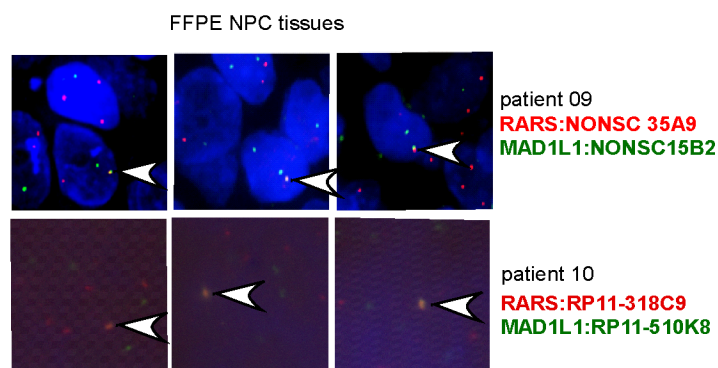
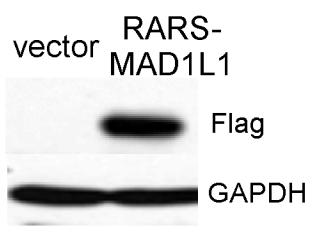
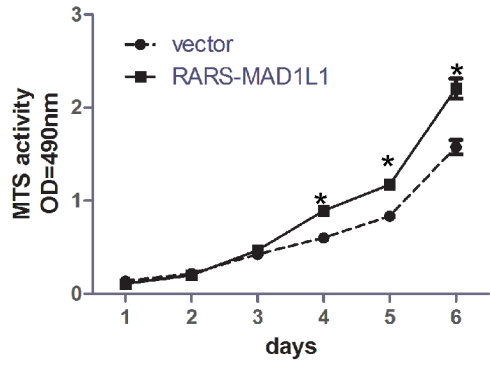


Figure 2

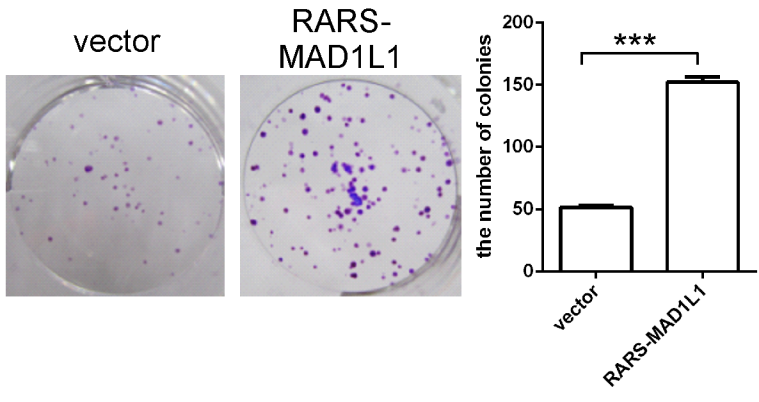
A



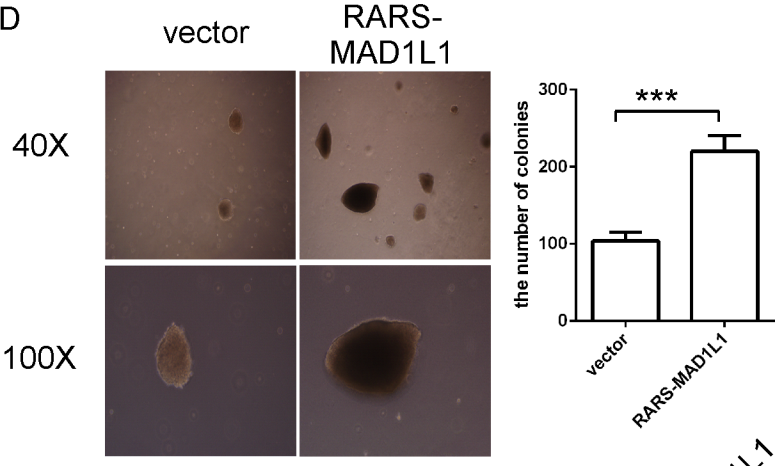
B



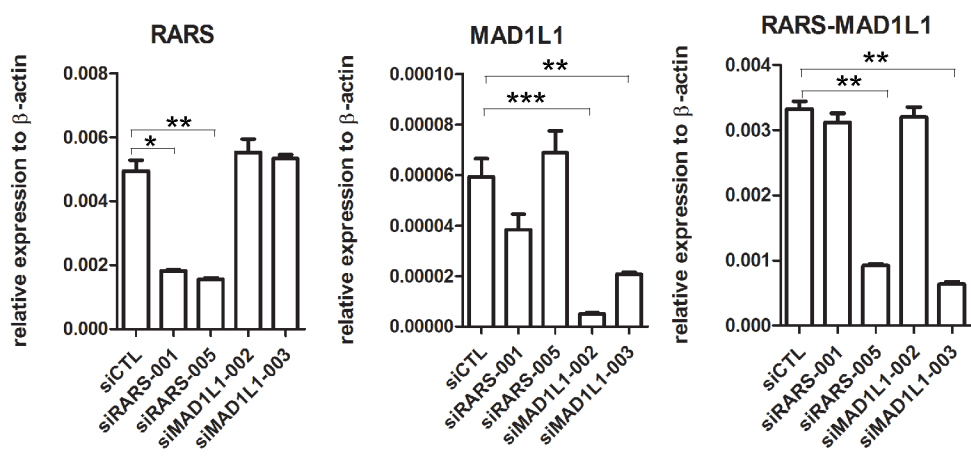
C



D



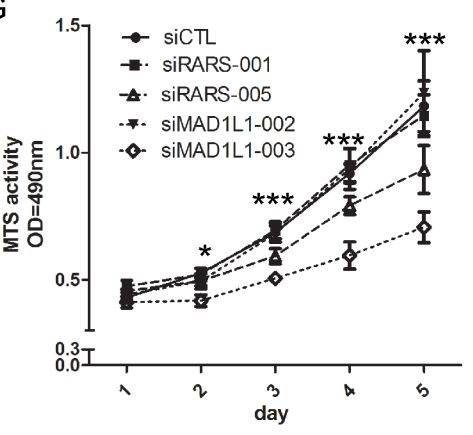
E



F



G



H

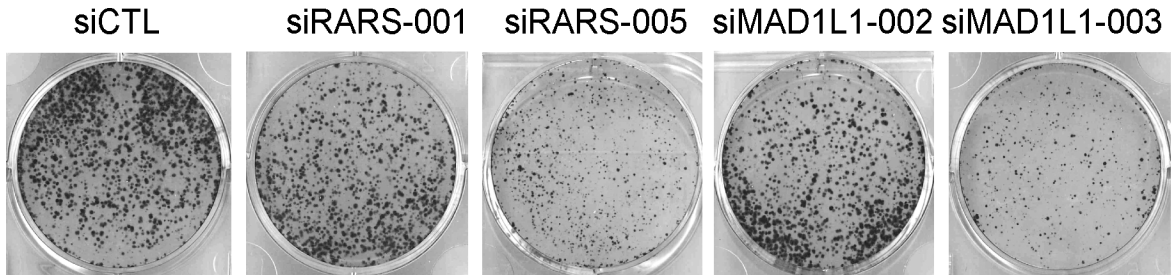


Figure 3

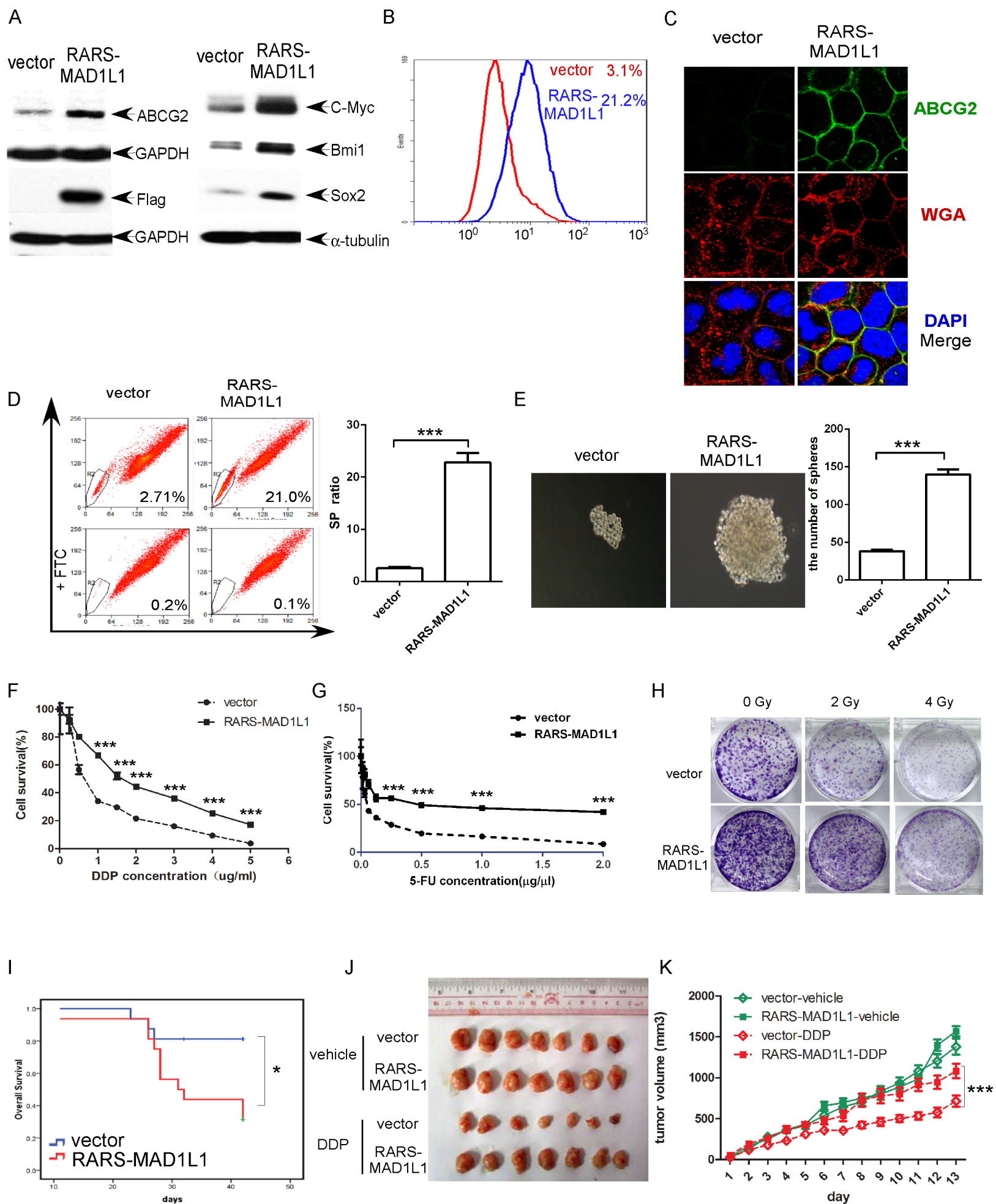


Figure 4

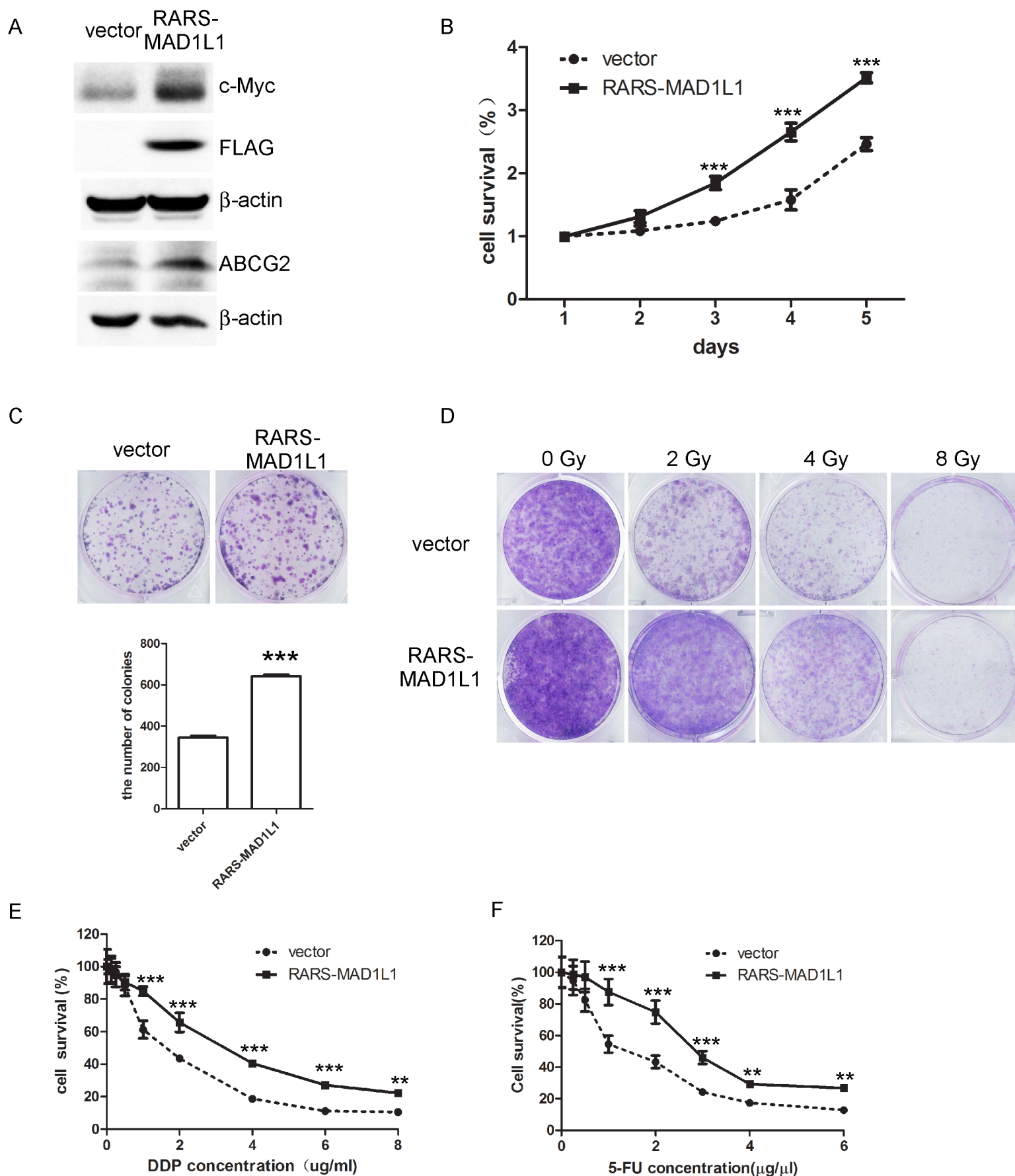
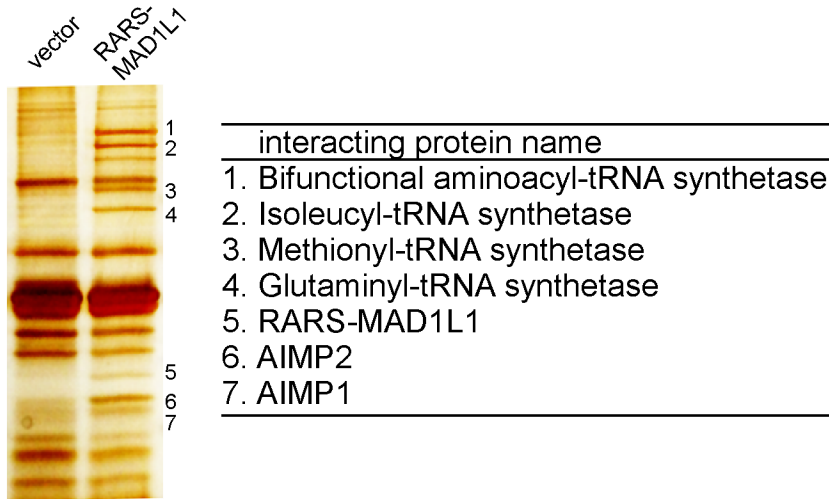
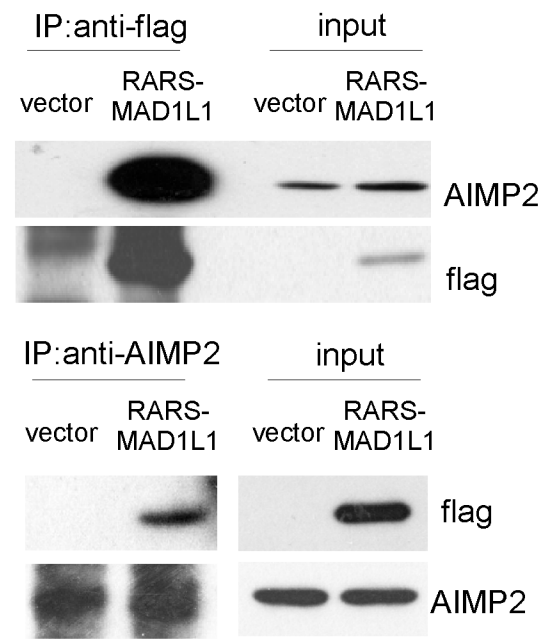


Figure 5

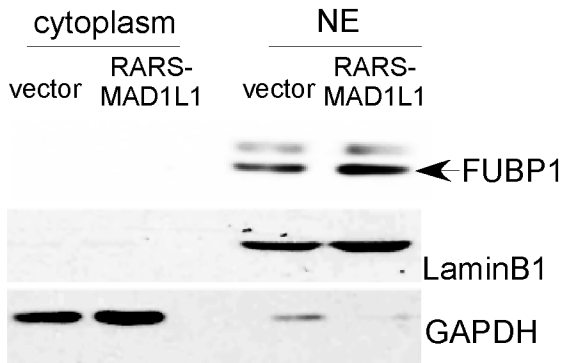
A



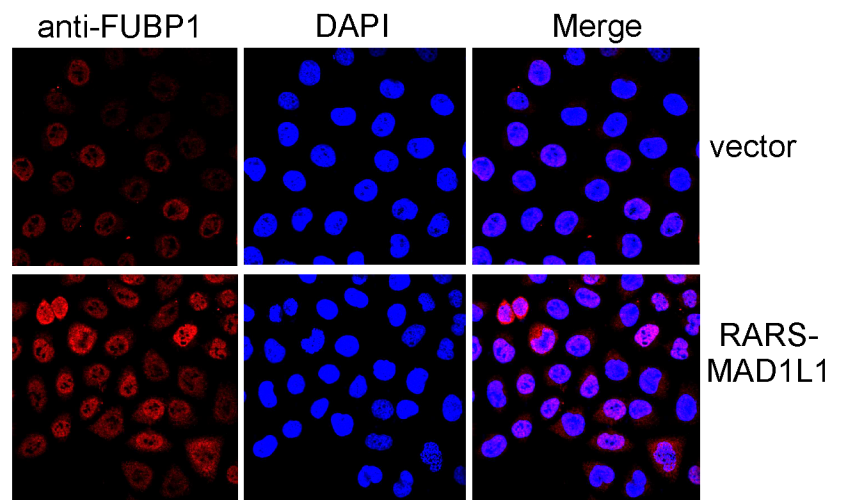
B



C



D



E

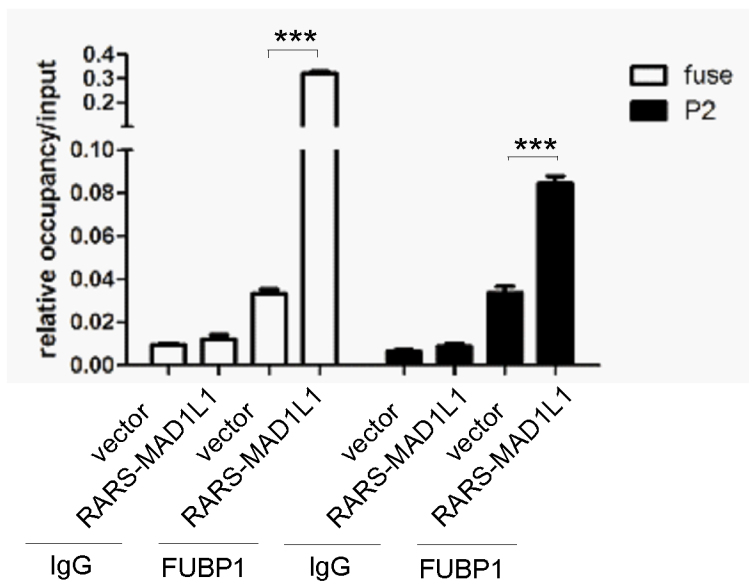
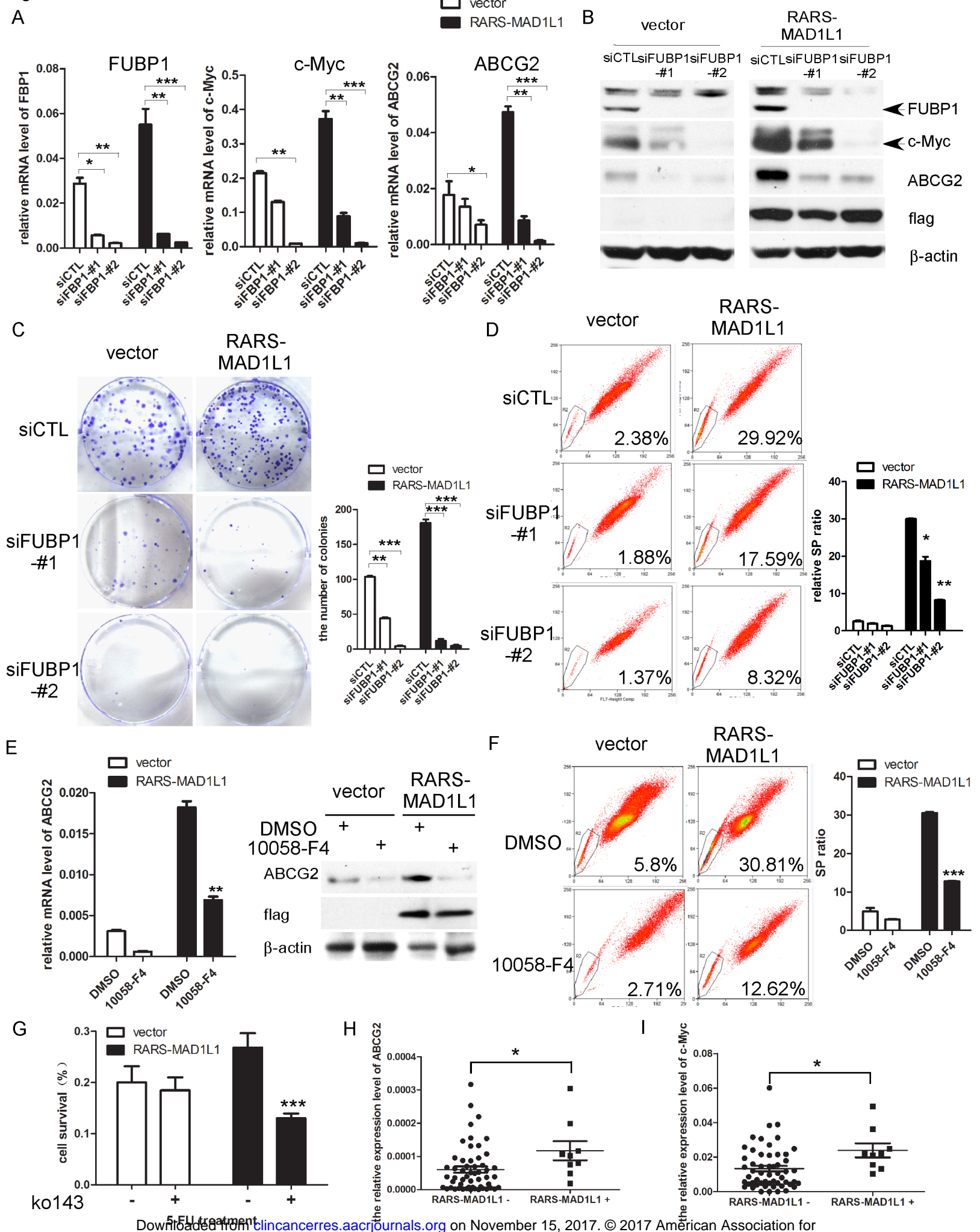


Figure 6



# Clinical Cancer Research

## The RARS-MAD1L1 Fusion Gene Induces Cancer Stem Cell-like Properties and Therapeutic Resistance in Nasopharyngeal Carcinoma

Qian Zhong, Zihua Liu, Zhi-Rui Lin, et al.

*Clin Cancer Res* Published OnlineFirst November 13, 2017.

<b>Updated version</b>	Access the most recent version of this article at: doi: <a href="https://doi.org/10.1158/1078-0432.CCR-17-0352">10.1158/1078-0432.CCR-17-0352</a>
<b>Supplementary Material</b>	Access the most recent supplemental material at: <a href="http://clincancerres.aacrjournals.org/content/suppl/2017/11/11/1078-0432.CCR-17-0352.DC1">http://clincancerres.aacrjournals.org/content/suppl/2017/11/11/1078-0432.CCR-17-0352.DC1</a>
<b>Author Manuscript</b>	Author manuscripts have been peer reviewed and accepted for publication but have not yet been edited.

<b>E-mail alerts</b>	<a href="#">Sign up to receive free email-alerts</a> related to this article or journal.
<b>Reprints and Subscriptions</b>	To order reprints of this article or to subscribe to the journal, contact the AACR Publications Department at <a href="mailto:pubs@aacr.org">pubs@aacr.org</a> .
<b>Permissions</b>	To request permission to re-use all or part of this article, use this link <a href="http://clincancerres.aacrjournals.org/content/early/2017/11/11/1078-0432.CCR-17-0352">http://clincancerres.aacrjournals.org/content/early/2017/11/11/1078-0432.CCR-17-0352</a> . Click on "Request Permissions" which will take you to the Copyright Clearance Center's (CCC) Rightslink site.